Autonomous Steering of Concentric Tube Robots for Enhanced Force/Velocity Manipulability

This paper appears in proceedings of 2019 IEEE/RSJ International Conference on Intelligent Robots and Systems (IROS) may change prior to publication. DOI: 10.1109/IROS40897.2019.8967593

Autonomous Steering of Concentric Tube Robots for Enhanced Force/Velocity Manipulability

Mohsen Khadem, John O'Neill, Zisos Mitros, Lyndon da Cruz*, Christos Bergeles*

***Abstract*—Concentric tube robots (CTR) can traverse tightly curved paths and offer dexterity in constrained environments, making them advantageous for minimally invasive surgical scenarios that experience strict anatomical and surgical constraints. Their shape is controlled via rotation and translation of several concentrically arranged super-elastic precurved tubes that form the robot backbone. As the elastic energy accumulated in the backbone due to bending and twist of the tubes increases, robots can exhibit sudden snapping motions, which can damage the surrounding tissues. In this paper, we proposed an approach for closed-loop steering of a redundant CTR that allows for snap-free motion and enhances its force/velocity manipulability, increasing the capacity of the robot to move and/or exercise forces along any direction. First, a controller stabilizes the CTR end-effector on a desired time-variant trajectory. Next, an online optimizer uses the robot's redundant Degrees of Freedom (DoF) to reshape its manipulability in real-time and steer it away from potentially snapping configurations or increase its capacity in delivering force payloads. Simulations and experiments demonstrate the performance of the proposed control strategy. The controller can steer a generally unstable CTR along trajectories while avoiding instabilities with a mean error of $850\,\mu$m, corresponding to 0.6% of arclength, and improves robot ability to exercise forces by 55%.**

I. Introduction

Concentric tube robots (CTR) can navigate confined spaces and conform to curvilinear paths, enabling them to reach and treat deeply-seated pathologies. Due to modelling uncertainties and mechanical instabilities associated with the design of a CTR, however, their stable control in constrained environments is a challenging task. It is possible that the ideal CTR architecture for a surgical scenario exhibits instabilities, termed "snapping", prohibiting their use within their entire workspace [1]. Further, it is possible that certain robot configurations exhibit suboptimal stiffness, therefore potentially causing damage as the robot traverses the anatomy, or be unable to exercise the forces required for tissue manipulation. In this paper, we propose a control strategy for accurate control and positioning of the tip of a generally unstable CTR by reshaping its unified force/velocity manipulability ellipsoid [2]. This way, the robot can follow desired trajectories while avoiding instabilities, and maximise its force application potential.

A CTR is a continuum robot with a backbone comprised of precurved elastic tubes. The shape of the backbone can be controlled via translation and rotation of the tubes with respect to each other. The mechanics-based model proposed in [3], [4] can be used to model the shape of the CTR as a function of robot's control inputs, *i.e.* tube rotations and translations, and external loading [5], [6].

Dexterity of the CTRs can be enhanced by employing tubes with higher precurvatures. Increasing tube precurvatures, however, increases the possibility of robot "snapping". "Snapping" is a mechanical instability caused by the rapid release of the elastic potential energy that is accumulated due to the bending and twisting of the tubes. Snapping, the unexpected swift change in the CTR's configuration, complicates smooth performance of tasks and can harm sensitive tissues in the proximity of the robot. In general, researchers have focused on ways to create CTRs without such instabilities, *i.e.* snap-free. Gilbert *et al.* [7] employed bifurcation theory to derive snap-free designs for unloaded CTRs. Xu *et al.* [8] presented an analytic stability condition for a CTR with several tubes with constant precurvatures. Till and Rucker improved the instability criterion to include the effects of dynamics [9]. Ha *et al.* [10] proposed two criteria to achieve elastic stability by employing optimal control theory, which were used to derive optimal design of a CTR without snapping issues. Others have focused on planning approaches to use unstable CTRs in their safe workspace. Bergeles *et al.*, [1] proposed a methodology for operating CTRs under anatomical constraints in their stable configuration via preoperative path planning. Similarly, Leibrandt *et al.* developed software for open-loop CTR control that avoids instabilities online [11]. The user is haptically directed towards precomputed paths that do not contain instabilities in real-time, but a static anatomy is assumed. Therefore, there is no opportunity to recover from user-enforced trajectories that lead to unstable configurations.

On-line stable and accurate trajectory-following control of CTRs remains a challenging task also when force application is considered. Most developed controllers assume that the CTR is stable by design and open-loop control strategies are used to steer the CTR [3], [12]. Closed-loop control strategies rely on the linear approximation of robot inverse kinematics near equilibrium [13]–[15] and try to avoid unstable paths via offline path planning. Further, limited effort has been invested on control that takes into account force application capabilities. One of few examples is the work in [16], which investigated stiffness control of surgical continuum manipulators.

In this paper, we propose a closed loop controller for autonomous steering of a CTR with real-time reshaping of the robot's unified force/velocity manipulability, recently introduced in [2]. We show capability for snapping avoidance

This research was supported by an ERC Starting Grant [714562].

M. Khadem (Corresponding author: mohsen.khadem@ed.ac.uk) is with the School of Informatics, University of Edinburgh, UK. J. O'Neill, Z. Mitros, and C. Bergeles are with the School of Biomedical Engineering and Imaging Sciences, King's College London, London, UK. L. da Cruz and Z. Mitros are with UCL Wellcome/EPSRC Centre for Interventional and Surgical Engineering Sciences, UCL. L. da Cruz is also with Moorfields Eye Hospital, London, UK. * denotes equal contribution.

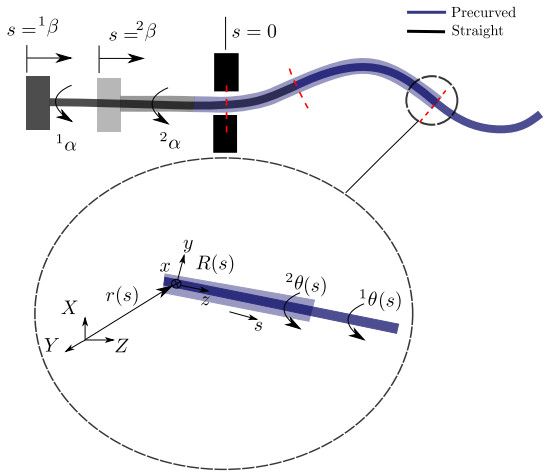

Fig. 1. Illustration of a concentric tube robot. Tubes are grasped at their respective proximal ends. The actuation variables $\alpha^i(t)$ and $\beta^i(t)$ denote the proximal base rotation and translation of the i-th tube, respectively. Each tube comprises a straight and a curved part. Angular displacement of tube i at arclength s is denoted by $\theta^i(s)$.

and force-application increase. We consider a CTR with three tubes and six control inputs (*i.e.* rotations and translations of three tubes). The selected robot is purposefully unstable at certain configurations within its workspace to showcase the capabilities of the proposed approach. As is normally considered in path following, the proposed controller uses the model-based Jacobian of the robot to minimize the Cartesian difference (3D without loss of generality) between the robot tip and the desired trajectory. The CTR is redundant, *i.e.* has more Degrees of Freedom (DoF) than what is required to track a 3D trajectory in Cartesian space. This enables implementation of control actions that retain the CTR tip on the desired 3D trajectory while allowing the orientation to change within the redundant workspace guided by secondary control tasks that aim to enhance robot manipulability.

II. Review of CTR Model

We start with a brief summary of the CTR model first presented in [3], [4]. The following notation is used throughout the paper: x, $\boldsymbol{x}$, and $\mathbf{x}$ denote a scalar, a vector, and a matrix, respectively. The prime, and dot, denote derivatives with respect to spatial coordinate s, and time t, respectively.

The CTR tubes are modelled as a deformable curve and a frame attached to every point along the curve's arc-length, with the z-axis of the frame tangent to the curve. The configuration of the robot can be defined using a set of 3D centroids along its arclength s, $\boldsymbol{r}(s) : [0, \ell] \to \mathbb{R}^3$, and a family of orthogonal transformations, $\mathbf{R}(s) : [0, \ell] \to SO(3)$ representing orientation change and twisting along s. Following the approach introduced in [3], [4], we can derive the constitutive equation for calculating the instantaneous curvature of the tubes and the overall robot shape. First, the robot is separated into transition points at which the continuity of shape and internal moment must be enforced (red dashed lines in Fig. 1). Each segment contains up N tubes, where N is the total number of tubes in the CTR. Next, we consider that the final deformed curve of all tubes at a given time t must be equal to the curve of the innermost tube $\boldsymbol{r}^i(s) = \boldsymbol{r}^1(s,t)$, as this is the one with the maximum extension (following the guidelines introduced in [3]). We use $\theta^i(s)$ to parametrize the tubes' twist around z axis, i.e., $\mathbf{R}^i(s) = \mathbf{R}^1(s)\mathbf{R}^{zi}_{\theta^i}(s)$, where $\mathbf{R}^{zi}$ denotes a rotation around the z axis of the i-th tube. Finally, based on these assumptions, in the absence of external torques, the curvature of tubes can be calculated as follows

$$\boldsymbol{r}^{1\prime} = \mathbf{R}^1 \boldsymbol{e}3, \tag{1a}$$

$$\mathbf{R}^{1\prime} = \mathbf{R}^1 \hat{\mathbf{u}}^1, \tag{1b}$$

$$u_n^{i\prime} = -\Big(\sum_{i=1}^{N} \mathbf{K}^i\Big)^{-1} \sum_{i=1}^{N} \mathbf{R}_{\boldsymbol{\theta}^i} \Big[\mathbf{K}^i\Big(\boldsymbol{u}^{i\prime} - \boldsymbol{U}^{i\prime}\Big) + \hat{\mathbf{u}}^i \mathbf{K}^i \big(\boldsymbol{u}^i - \boldsymbol{U}^i\big)\Big] - \Big(\sum_{i=1}^{N} \mathbf{K}^i\Big)^{-1} \Big[\boldsymbol{e}3 \times \mathbf{R}^{1T} \int_0^s \boldsymbol{f}(\epsilon, t) \mathrm{d}\epsilon\Big]\Big|_{n=1,2} \tag{1c}$$

$$u_3^{i\prime} = \frac{E^i I^i}{G^i J^i}(u_1^i U_2^i - u_2^i U_1^i), \tag{1d}$$

$$\theta^{i\prime} = u_3^i, \tag{1e}$$

where superscript $i = 1, \cdots, N$ denotes the i-th tube, with $i = 1$ corresponding to the innermost tube; subscript $n = 1, 2, 3$ denotes the n-th element of a vector; $\boldsymbol{e}3 = [0,\ 0,\ 1]^T$ is the unit vector aligned with the z-axis of the global coordinate frame; $\boldsymbol{u}$ is the curvature vector of the deformed backbone of the robot; denotes the precurvature of each tube $\boldsymbol{U}^i$ denotes the precurvature of each tube in its reference configuration; θ^i denotes the angle of twist about the local z-axis with respect to global frame; $\mathbf{K}^i = \mathrm{diag}(E^i I^i, E^i I^i, G^i J^i)$ is the stiffness matrix for tube i; E is the tube's Young's modulus; I is the second moment of inertia; G is the shear modulus; J is the polar moment of inertia; $\boldsymbol{f}$ is any external force applied to the robot. Please note that we drop the (s) notation for simplicity.

The boundary conditions can be specified in terms of tube curvature and the actuators' values as follows

$$\begin{aligned} \boldsymbol{r}^1\big|_{s=0} &= [0\ 0\ 0]^T, \quad & \mathbf{R}^1\big|_{s=0} &= \mathbf{R}^{z1}_{(\alpha^1 - \beta^1 u_3^1)}, \\ \theta^i\big|_{s=0} &= \alpha^i - \beta^i u_3^i, & \boldsymbol{u}^i\big|_{s=\ell^i+\beta^i} &= \boldsymbol{U}^i, \end{aligned} \tag{2}$$

where the notation $(\big|_{s=\xi})$ indicates the value of a variable at arclength of ξ, and ℓ^i is the length of the i-th tube. Solving (1) and (2) gives the robot backbone curvature and shape.

III. Control Architecture

We design a controller to track a time-varying desired trajectory, $\boldsymbol{x}_d(t)$. Without loss of generality, we assume that the CTR is composed of three tubes and that the end-effector is the tip of the inner most tube, denoted by $\boldsymbol{x}(t) = \boldsymbol{r}^1\big|_{s=\ell^1+\beta^1}$.

First, we define the Jacobian matrix, $\mathbf{J}$, that maps the joint velocities, $\boldsymbol{q} \in \mathbb{R}^6$, to the robot end-effector velocity, $\boldsymbol{x} \in \mathbb{R}^3$, as

$$\dot{\boldsymbol{x}} = \mathbf{J}\dot{\boldsymbol{q}}, \tag{3}$$

where $\mathbf{J}$ is the 3×6 Jacobian matrix and $\boldsymbol{q}$ is the actuator value vector and consists of the rotations and translations of each

tube, i.e., $\alpha^i(t)$ and $\beta^i(t)$, as shown in Fig. 1. We numerically estimate the Jacobian as

$$\mathbf{J} = \frac{\Delta \boldsymbol{x}}{\Delta \boldsymbol{q}} = \begin{bmatrix} \frac{\boldsymbol{x}^T(\boldsymbol{q} + \frac{\Delta q_1}{2}\boldsymbol{e}_1) - \boldsymbol{x}^T(\boldsymbol{q} - \frac{\Delta q_1}{2}\boldsymbol{e}_1)}{\Delta q_1} \\ \dots \\ \frac{\boldsymbol{x}^T(\boldsymbol{q} + \frac{\Delta q_n}{2}\boldsymbol{e}_n) - \boldsymbol{x}^T(\boldsymbol{q} - \frac{\Delta q_n}{2}\boldsymbol{e}_n)}{\Delta q_n} \end{bmatrix}^T \tag{4}$$

where $\boldsymbol{e}_i$ is the ith unit vector of the canonical basis of the 6-dimensional joint space. From various methods for estimating the Jacobian, we select the above formulation as it gives rise to parallelisable computations without sacrifices in the kinematics model's accuracy [17].

According to [18], the general inverse kinematics of the CTR in (3) can be written as

$$\dot{\boldsymbol{q}} = \mathbf{J}^\dagger \dot{\boldsymbol{x}} + (\mathbf{I} - \mathbf{J}^\dagger \mathbf{J})\dot{\boldsymbol{q}}_0, \tag{5}$$

where $\mathbf{J}^\dagger$ is the pseudo-inverse of Jacobian, $\mathbf{I}$ is the 6×6 identity matrix and $\dot{\boldsymbol{q}}_0$ is a 6×1 arbitrary joint velocity vector. The second term in (5) is the projection operator of $\dot{\boldsymbol{q}}_0$ in the null-space of the mapping $\mathbf{J}$. Thus, $\dot{\boldsymbol{q}}_0$ produces motions of the CTR backbone without affecting the tip.

In this section we employ the inverse kinematics of (3) to design a controller to steer the CTR. Assuming the desired trajectory, $\boldsymbol{x}_d(t)$, is known, desired joint variables, $\boldsymbol{q}_d(t)$, to follow that trajectory can be estimated via the first term in (5). Solutions of joint variables estimated only using (5), however, lead to significant errors due to modelling uncertainties and system nonlinearities affecting the estimation of Jacobian in (4). Considering that the error between the desired trajectory and actual trajectory of the robot is $\boldsymbol{e} = \boldsymbol{x}_d - \boldsymbol{x}$, one can use the following control law to regulate the error to zero [19]:

$$\dot{\boldsymbol{q}}_d = \mathbf{J}^\dagger[\dot{\boldsymbol{x}}_d + \mathbf{K}(\boldsymbol{x}_d - \boldsymbol{x})], \tag{6}$$

where $\boldsymbol{q}_d$ is the desired actuator velocities and the proportional gain, $\mathbf{K}$, is a symmetric positive definite matrix. Substituting (3) in (6) one obtains $\dot{\boldsymbol{e}} + \mathbf{K}\boldsymbol{e} = 0$, which asymptotically stabilizes the error to zero.

Combining (6) and (5) the general inverse solution of CTR can be obtained as

$$\dot{\boldsymbol{q}} = \mathbf{J}^\dagger[\dot{\boldsymbol{x}}_d + \mathbf{K}(\boldsymbol{x}_d - \boldsymbol{x})] + (\mathbf{I} - \mathbf{J}^\dagger \mathbf{J})\dot{\boldsymbol{q}}_0. \tag{7}$$

Figure 2 shows the block diagram of the proposed control strategy based on (7). In the next Section, we will employ the robot self motion, $\boldsymbol{q}_0$, to optimize the manipulability of the CTR with the aim of snapping avoidance.

IV. Velocity Manipulability and Snapping Avoidance

Based on (7), one can exploit the motion of the robot in its null space by modulating $\boldsymbol{q}_0$ to perform a secondary task alongside the primary task of trajectory tracking. A typical approach for null space controller is a gradient function of the form

$$\dot{\boldsymbol{q}}_0 = -\upsilon \frac{\partial \mathcal{C}(\boldsymbol{q})}{\partial \boldsymbol{q}} \tag{8}$$

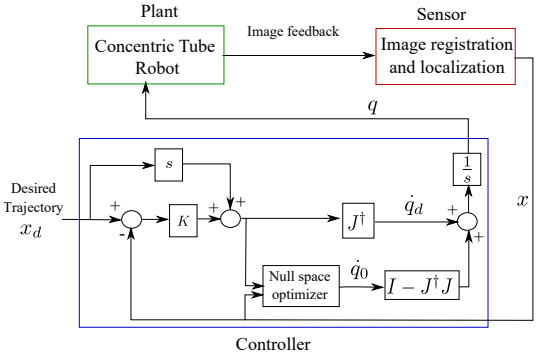

Fig. 2. Block diagram of the control loop.

where $\upsilon > 0$ and $\mathcal{C}(\boldsymbol{q})$ is a scalar cost function that we would like to minimize.

We propose to optimize a cost function based on the definition of manipulability. Manipulability describes the characteristics of feasible motions in the task space corresponding to unit joint velocity vectors. However, the classic definition of manipulability cannot be used for flexible continuum robots. Unlike rigid-link robots, where the pose of any point on the robot can be fully defined by link lengths and joint angles, the pose of a continuum robot is a function of the manipulator's shape and elasticity.

Therefore, we use the measure of manipulability of continuum robots developed in our previous work [2]. It considers the inherent compliance of the continuum robot, and can be used to estimate optimal direction for applying velocity and force when the robot end-effector is under external forces.

The unified force-velocity manipulability ellipsoid is defined as

$$\text{UME} = \{\dot{\boldsymbol{x}} : \| \dot{\boldsymbol{q}} \| = 1 \ \& \ \Lambda = \text{const.}\}, \tag{9}$$

where Λ denotes the desired stiffness at the robot end-effector. The developed force-velocity manipulability considers robot compliance and adheres to the force-velocity duality generally associated with rigid-link robots, *i.e.* a direction along which good velocity manipulability is obtained, is normal to the optimal direction with good force manipulability.

Following the approach presented in [2], the unit sphere in the joint velocity space $\dot{\boldsymbol{q}}$ can be mapped onto the robot velocity in the task space via

$$\mu = \mathbf{C}^T \Lambda^T \mathbf{J}\mathbf{J}^T \Lambda \mathbf{C}, \tag{10}$$

where $\mathbf{C}$ is the Compliance matrix defined as

$$\mathbf{C} = \frac{\Delta \boldsymbol{x}}{\Delta \boldsymbol{f}} = \begin{bmatrix} \frac{\boldsymbol{x}^T(\boldsymbol{f} + \frac{\Delta f_1}{2}\boldsymbol{e}_1) - \boldsymbol{x}^T(\boldsymbol{f} - \frac{\Delta f_1}{2}\boldsymbol{e}_1)}{\Delta f_1} \\ \dots \\ \frac{\boldsymbol{x}^T(\boldsymbol{f} + \frac{\Delta f_3}{2}\boldsymbol{e}_3) - \boldsymbol{x}^T(\boldsymbol{f} - \frac{\Delta f_3}{2}\boldsymbol{e}_3)}{\Delta f_3} \end{bmatrix}^T \tag{11}$$

In derivation of (10) we assumed that external torques on the robot are zero. Now, based on (10) the UME ellipsoid denoted by μ can be spanned by a set of principal axes $\lambda_i \boldsymbol{z}_i$ where

λ_i and $\boldsymbol{z}_i$ are the singular values and left-singular vectors of matrix $\mathbf{C}^T\Lambda^T\mathbf{J}$ estimated via singular value decomposition.

Based on the definition of instability for CTRs from [8], the robot may become unstable as the mapping from joint space to robot task space (*i.e.* the Jacobian) becomes rank deficient and the solution of the forward kinematics becomes non-unique (sufficient condition). This happens when the singular values of the Jacobian become very small.

We argue that via reshaping the manipulability ellipsoid of the CTR toward a sphere during trajectory tracking, we can ensure the rank efficiency of the CTR Jacobian and uniqueness of the forward kinematics solution. This will enable stable snap-free control of the CTR. Also, reshaping the UME enables the CTR to avoid the limits of its workspace where its manipulability is minimal. We can also extend the manipulability ellipsoid perpendicular to the direction of applied forces to enhance robot ability to apply an external force to a fixed object.

Based on the above argument, we define the secondary task cost function, $\mathcal{C}$, as the difference between the manipulability ellipsoid μ and a desired manipulability denoted by μ_d. In (10), μ is a symmetric positive definite (SPD) function of $\boldsymbol{q}$. Measuring distances between two SPD matrices is often nontrivial as the distance function must respect the non-Euclidean geometry of SPD matrices. Here, we employ the SPD metric introduced in [20], which respects non-Euclidean geometry, is computationally efficient, and forms a convex problem. The cost function can be defined as

$$\mathcal{C} = \log|\frac{\mu+\mu_d}{2}| - \frac{1}{2}\log|\mu\mu_d|. \tag{12}$$

Estimating $\mathcal{C}$ requires only computation of determinants, which can be done rapidly via 3 Cholesky factorizations. The evaluation of gradient of $\mathcal{C}$ with respect to q is required to solve (8). It can be estimated as $\dfrac{\partial\mu}{\partial\boldsymbol{q}}((\mu+\mu_d)^{-1} - \frac{1}{2}\mu^{-1})$. Based on (10), estimating $\dfrac{\partial\mu}{\partial\boldsymbol{q}}$ requires calculating the Hessian of $\boldsymbol{x}$ with respect to $\boldsymbol{f}$ and $\boldsymbol{q}$. We implemented BFGS algorithm [21] to estimate the Hessians as a function of the Compliance and Jacobian matrices iteratively.

As mentioned previously, the desired manipulability can be maximized along a desired direction to increase the CTR's force capability. Based on the force-velocity duality, if $\boldsymbol{a} \in R^3$ is the unit vector that indicates the direction of external forces, we can maximize CTR force capability by minimizing the UME in the direction of $\boldsymbol{a}$. By using singular value decomposition (SVD), $\boldsymbol{a}$ can be decomposed as $\boldsymbol{a} = \mathbf{U}\boldsymbol{\Sigma}V^T$, where U is 3×3 unitary matrix, Σ is an 3×1 vector in which non zero value is known as the singular value of $\boldsymbol{a}$, and V is a scalar. The desired UME is a circle with small thickness in the direction of $\boldsymbol{a}$ and can then be defined as

$$\mu_d = U\begin{bmatrix}\nu\Sigma, & \begin{bmatrix}\boldsymbol{0}_{1\times2}\\ \mathbf{I_{2\times2}}\end{bmatrix}\end{bmatrix}U^{-1} \tag{13}$$

where $\mathbf{I}$ is an identity matrix, $\boldsymbol{0}_{1\times2}$ is a vector of zeroes, and $0 < \nu < 1$ is a scalar scaling factor that defines the length of the minor axes of the μ_d. In theory, an ideal velocity manipulability μ_d is a circle (*i.e.* $\nu = 0$) with zero length in the direction of $\boldsymbol{a}$, corresponding to maximum force manipulability capability in that direction. However, such a UME is rank deficient and causes the CTR to move toward a singular configuration and snap. Therefore, the parameter ν needs to be small but non-zero to avoid singularity in any direction.

The joint limits also have a major impact on the robot end-effector workspace. To consider their effect, we use the constrained Jacobian $\mathbf{J}^c$ [22] that is formed by actively penalizing the columns of the matrices individually using

$$\mathbf{J}_i^c = P_i^c\mathbf{J}_i, \tag{14}$$

where J_i is the i^{th} column of the robot Jacobian, and P_i^c is the joint-wise penalization function given by

$$P_i^c = \frac{1 - exp(\frac{-4k_c(q_i-q_{i,min})(q_{i,max}-q_i)}{(q_{i,max}-q_{i,min})^2})}{1-exp(-k_c)} \tag{15}$$

where the coefficient "4" and the denominator "$1-exp(-k_c)$" in (15) is needed to normalize the penalization term such that P_i^c spans the interval $[0,1]$. Using this penalty function, the individual columns of $\mathbf{J}$ and $\mathbf{C}$ are penalized when the ith joint value q_i approaches the limits $q_{i,min}$ or $q_{i,max}$. Now, by substituting the constrained Jacobian $\mathbf{J}^c$ in (10) we can consider the robot's mechanical constraints and ensure that the base of the tubes will not collide with each other or pass the entry point.

In the next section, a simulation study is performed to evaluate the performance of the proposed manipulability reshaping approach.

V. Simulation Study

Results of a simulation study using the proposed controller are presented. The initial position of robot tubes, β^i, are -0.2858, -0.2025, and -0.0945 mm. The initial angle of all tubes, θ^i, are $\pi/2$. The controller parameters used were $\mathbf{K} = 5\mathbf{I}$, and $\upsilon = 0.05$; λ, in (16) was selected as 0.5. These values were selected following simulations to achieve the minimum tracking error. The controllers are tested on a perturbed CTR model with $\pm10\%$ uncertainty in the values of the tubes' Young and shear moduli with respect to the nominal ones. The CTR design parameters are shown in Table I. For consistency, these parameters are identical to those used in our experimental setup in Sec. VI. The selected robot is purposefully unstable within its workspace to test the performance of the controller in avoiding snapping.

The performance of the proposed controller is compared to two other controllers:

1) A controller given by (6) that uses Jacobian without null-space optimizer.
2) A controller using damped least-squares inverse kinematics.

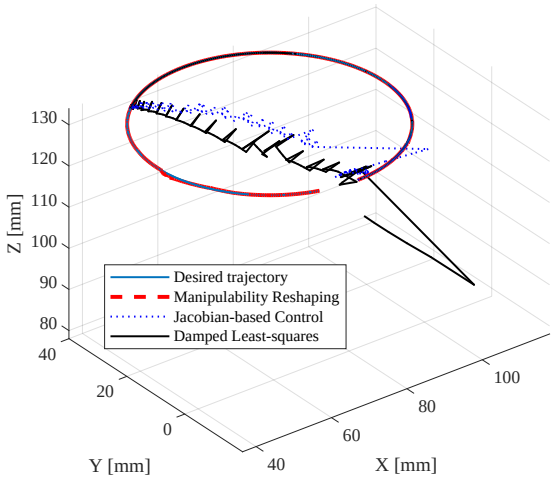

(a)

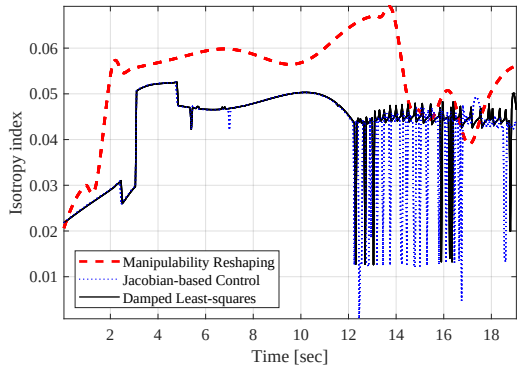

(b)

Fig. 3. Simulation results for CTR steering on a circular trajectory in 3 scenarios. (a) A comparison between the desired trajectory and actual trajectory. (b) A comparison of the isotropy index.

The damped least-squares is an effective strategy that allows Jacobian-based control of robots in the neighborhood of kinematic singularities [23]. In this case, the pseudo-inverse of the robot Jacobian in (6) can be replaced by

$$(\mathbf{J}^T\mathbf{J} + \lambda^2\mathbf{I})^{-1}\mathbf{J}^T \tag{16}$$

where λ is the damping factor and improves inverse kinematic when Jacobian is ill-conditioned and close to a singularity.

In the simulation study, a circular trajectory near the limits of the robot workspace was selected. The simulation results are shown in Fig. 3.

It can be seen from Fig. 3 that the Jacobian-based controller and damped least-squares controller are unable to track the desired trajectory and eventually snap, while Fig. 4 shows that joint constraints are also violated (the 3rd and 2nd tubes collide). The controller using manipulability reshaping is able to follow the desired trajectory while avoiding snapping and satisfying joint constraints. Figure 3(b) shows a comparison of isotropy index defined as $\epsilon = \frac{\sigma_{min}(\mathbf{J})}{\sigma_{max}(\mathbf{J})}$ between the three controllers, where σ_{max} and σ_{min} are maximal and minimal singular values of $\mathbf{J}$. Small values of ϵ indicate that the

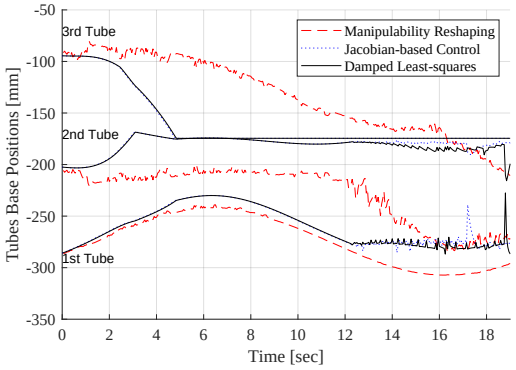

(a)

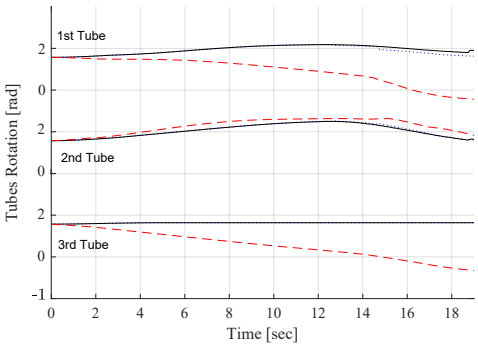

(b)

Fig. 4. Comparison between (a) position of the base of robot's tubes, and (b) rotation of the tubes for 3 simulated scenarios.

Jacobian is ill-conditioned. As can be seen, the proposed controller is able to increase the isotropy index to steer away from singularities.

In the next section, experiments are performed to assess the practical performance of the proposed controller.

VI. Experiments and Discussion

The setup used in the experiments is shown in Fig. 5. In order to measure the CTRs tip location we used two calibrated Logitech HD Pro C930e Webcams set up orthogonally to capture the position of the tip of the CTR. The cameras were running at 1080p resolution and 30 frames per second. The camera capture and analysis used ROS [24] and OpenCV [25]. Each camera used two threads, one for video capture and one for video analysis. A 4-core PC was used to allow each major thread its own core. A spherical coloured marker was placed at the tip of the CTR and the cameras filtered out its colour by thresholding in the Hue/Saturation/Value (HSV) colour space. The centroid of the largest contiguous blob was then found, giving a vector from each camera's origin to the marker.

Each camera had an asymmetric circular calibration grid within the field of view, which gave the pose of the camera relative to the grid. An average of 30 poses was taken on startup, after which point the grid was no longer monitored to allow the fastest possible processing of the marker. A manual backbone segmentation mode was also used for establishing the base and shape of the CTR relative to the calibration grid.

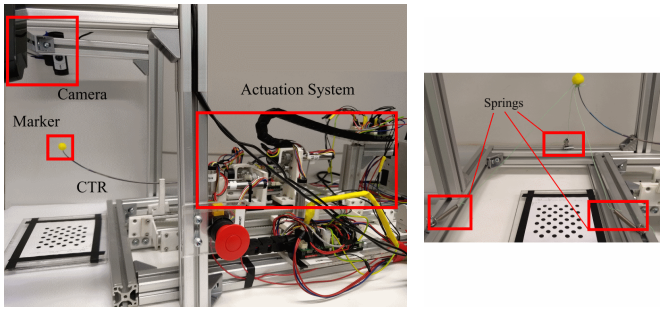

(a) (b)

Fig. 5. (a) Experimental setup used to validate the controller. The CTR is composed of three precurved Nitinol tubes. Two calibrated cameras are used to measure the position of the CTR. (b) Several springs with the stiffness of 0.154 N/mm are connected to the robot tip to apply external forces to the robot in various directions.

TABLE I
PHYSICAL PARAMETERS FOR CTR'S TUBES.

	Tube 1	Tube 2	Tube 3
Inner Radius [mm]	0.35	0.7	1
Outer Radius [mm]	0.55	0.9	1.2
Straight Length [mm]	431	330	174
Curved Length [mm]	103	113	134
Curvature [m$^-$1]	21.3	13.1	3.5
Young's Modulus, E [GPa]	10.25	68.6	16.96
Shear Modulus, G [GPa]	18 .79	11.53	14.25

This was done by clicking on backbone points in each image, and then using triangulation to extract the 3D point cloud.

For the real-time tip tracking, two-view triangulation was calculated by a dedicated thread and re-evaluated for each new frame from either camera, since the camera shutters were not synchronized.

A set of experiments was performed to calibrate the CTR model parameters, namely, Young's and shear moduli of the tubes. The parameters are identified by fitting the kinematic model given in (1) to the shape of the robot estimated via the cameras at 25 different configurations. The identified parameters of the model are given in Table I; recall that this robot is also used in our simulations for consistency. The maximum error of the model in predicting the CTR tip position was 1.74 cm, while the mean error per length of the robot was 9%, in accordance with modelling errors per arclength reported in the literature [4].

The identified mechanics model was implemented in the controller discussed in Sec. III and Sec. IV to steer the CTR. An Intel Core i7 (2.93 GHz) machine was used to solve the optimal problem at sampling time of 50 ms. Using simulations, parameters of the controller were identified as $\mathbf{K} = 5\mathbf{I}$ and $\upsilon = 0.05$. The active limits on the control inputs that were used to penalize the Jacobian are

$$\begin{aligned} \boldsymbol{q}_{min} &= [-\beta_{min} - \epsilon,\ \beta^1 + \epsilon,\ \beta^2 + \epsilon]^T, \\ \boldsymbol{q}_{max} &= [\beta^2 - \epsilon,\ \beta^3 - \epsilon,\ 0]^T, \end{aligned} \tag{17}$$

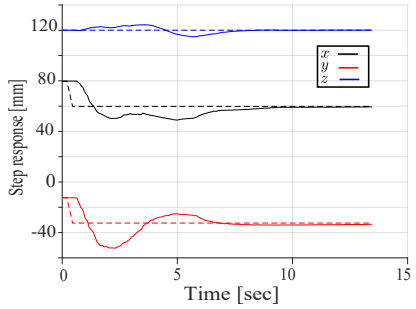

Fig. 6. Representative experimental results for CTR tip position in response to a step input.

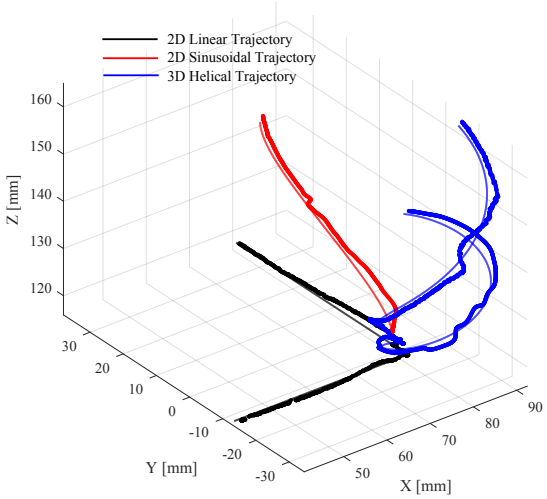

Fig. 7. Experimental results for trajectory tracking. Desired and actual trajectory are shown with thin and thick lines, respectively.

where $\beta_{min} = 300$ mm is the maximum possible distance of the first tube (i.e, inner most tube) from the entry point and $\epsilon = 10$ mm is the desired offset between the proximal end of the tubes. Constraints in (17) ensure the bases of the tubes will not collide with each other or pass the entry point.

In the first experiment, the CTR was commanded to reach a given point in 3D space. We evaluated the response of the control system to 3D step inputs in the range of 10 to 25 mm. Representative results for step response experiments are shown in Fig. 6. The mean error, defined as the Cartesian difference between the desired and actual position of CTR end-effector, for 10 trials was 0.28 mm, corresponding to 0.18% of arclength.

In the next experiment, we evaluated the performance of the controller in tracking various trajectories including linear, sinusoidal, and helical ones. 10 trajectories were selected for each scenario. Representative results are shown in Fig. 7. The root mean squared error of the tracking scenario was 850 μm. The root-mean-squared error is calculated as $\text{RMSE}_x = \sqrt{\frac{\sum_{i=1}^{n}(\|\boldsymbol{x}_d\|_i - \|\boldsymbol{x}\|_i)^2}{n}}$, and is used as a measure of the differences between the desired trajectory, $\boldsymbol{x}_d$, and the actual trajectory that was experimentally observed, *i.e.* $\boldsymbol{x}$, for n

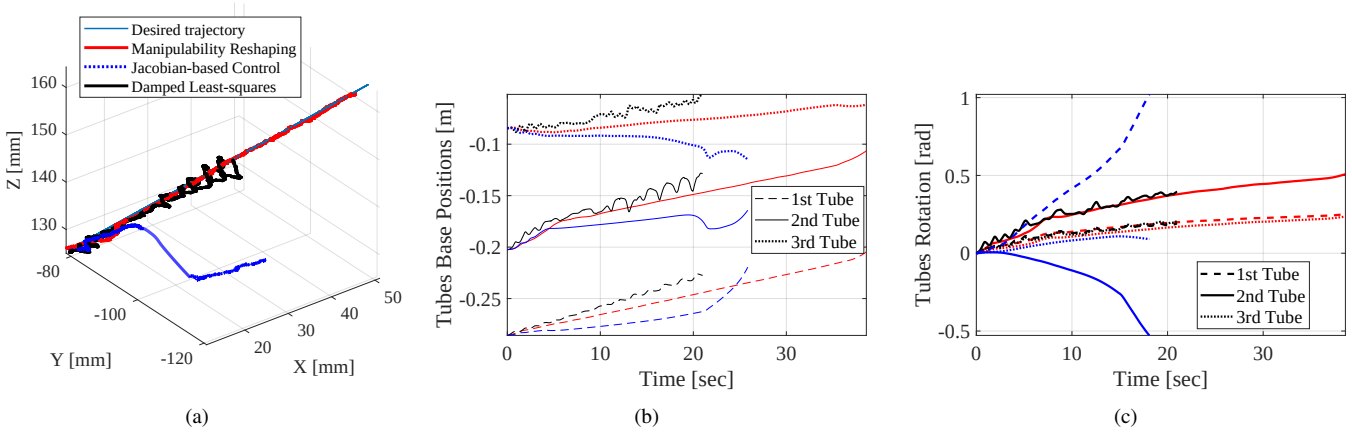

Fig. 8. Experimental results for CTR steering on a 3D line in 3 scenarios. (a) A comparison between the desired trajectory and actual trajectory for Jacobian-based control, controller with manipulability reshaping, and controller with least damped-squares inverse kinematics. (b) A comparison of the position of base of robot's tubes. (c) A comparison of the angular position of base of robot's tubes.

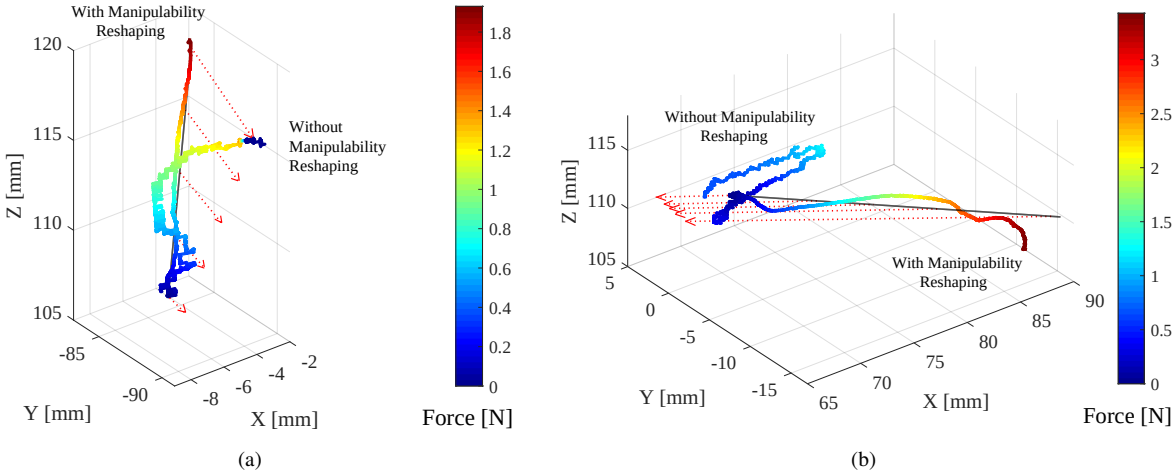

Fig. 9. Representative experimental results with external force applied to the CTR end-effector. Results are presented for controllers with and without manipulability reshaping. Black line denotes the desired trajectory. Direction of external force applied by the springs along the desired trajectory is shown with red dashed line.

sampling times. The maximum tracking error was $5.6\,\text{mm}$ throughout all experiments, and occurred when tracking a helical trajectory.

In the next experiment, we evaluated the performance of the controller in avoiding snapping. The CTR was steered on a 3D trajectory near its joints' limits. Results are shown in Fig. 8. It can be seen that the controller without snapping avoidance indeed becomes unstable. The damped least-squares controller is able to track the desired trajectory but as shown in Fig. 8(b) the joint constraints defined in (17) are violated (the 3^{rd} tubes reaches the entry point). However, the proposed control system with snapping avoidance can avoid CTR snapping by constantly reshaping the robot manipulability via modulating control inputs in robot null space. The isotropy index recorded for manipulability reshaping, Jacobian-based, and damped least-squares controllers were 0.0401, 0.0101, and 0.007, respectively.

In the last experiment, the performance of the controller in following trajectories under external forces was evaluated. Several springs with stiffness of 0.154 N/mm were connected to the robot tip to apply external forces along various directions (see Fig. 5). The controller parameters for force tracking, ν in (13) and Λ, in (9) were 0.15 and $0.0015\mathbf{I}$. Results presented in Fig. 9 show that the proposed controller can apply more force than the simple Jacobian-based controller without manipulability reshaping. Based on 10 experimental trials performed, the proposed controller improves robot force capability by 55% compared to the Jacobian-based controller.

VII. Concluding Remarks

In this paper, we proposed a closed-loop controller for autonomous steering of CTRs on desired trajectories. The proposed controller is capable of stable steering of CTR end-effector via real-time reshaping of the manipulability of the robot. Experimental results demonstrate the accuracy and performance of the controller in following desired trajectories and avoiding CTR snapping. The mean error of the proposed controller in trajectory tracking was $0.85\,\text{mm}$.

In future work, we will improve the accuracy of the proposed controller by enhancing the computational efficiency of the controller, which we believe can be achieved by parallel computation of the manipulability-based cost function without sacrifices in the controller accuracy.

REFERENCES

[1] C. Bergeles, A. H. Gosline, N. V. Vasilyev, P. J. Codd, P. J. del Nido, and P. E. Dupont, "Concentric tube robot design and optimization based on task and anatomical constraints," *IEEE Transactions on Robotics*, vol. 31, no. 1, pp. 67–84, 2015.

[2] M. Khadem, L. da Cruz, and C. Bergeles, "Force/velocity manipulability analysis for 3d continuum robots," in *IEEE/RSJ International Conference on Intelligent Robots and Systems (IROS)*, 2018, pp. 4920–4926.

[3] P. E. Dupont, J. Lock, B. Itkowitz, and E. Butler, "Design and control of concentric-tube robots," *IEEE Transactions on Robotics*, vol. 26, no. 2, pp. 209–225, 2010.

[4] R. J. Webster, J. M. Romano, and N. J. Cowan, "Mechanics of precurved-tube continuum robots," *IEEE Transactions on Robotics*, vol. 25, no. 1, pp. 67–78, 2009.

[5] D. C. Rucker, B. A. Jones, and R. J. W. III, "A geometrically exact model for externally loaded concentric-tube continuum robots," *IEEE Transactions on Robotics*, vol. 26, no. 5, pp. 769–780, 2010.

[6] J. Lock, G. Laing, M. Mahvash, and P. E. Dupont, "Quasistatic modeling of concentric tube robots with external loads," in *2010 IEEE/RSJ International Conference on Intelligent Robots and Systems*, 2010, pp. 2325–2332.

[7] H. B. Gilbert, R. J. Hendrick, and R. J. W. III, "Elastic stability of concentric tube robots: A stability measure and design test," *IEEE Transactions on Robotics*, vol. 32, no. 1, pp. 20–35, 2016.

[8] R. Xu, S. F. Atashzar, and R. V. Patel, "Kinematic instability in concentric-tube robots: Modeling and analysis," in *5th IEEE RAS/EMBS International Conference on Biomedical Robotics and Biomechatronics*, 2014, pp. 163–168.

[9] J. Till and D. C. Rucker, "Elastic stability of cosserat rods and parallel continuum robots," *IEEE Transactions on Robotics*, vol. 33, no. 3, pp. 718–733, 2017.

[10] J. Ha, F. C. Park, and P. E. Dupont, "Optimizing tube precurvature to enhance the elastic stability of concentric tube robots," *IEEE Transactions on Robotics*, vol. 33, no. 1, pp. 22–37, 2017.

[11] K. Leibrandt, C. Bergeles, and G. Yang, "Concentric tube robots: Rapid, stable path-planning and guidance for surgical use," *IEEE Robotics Automation Magazine*, vol. 24, no. 2, pp. 42–53, 2017.

[12] H. B. Gilbert, J. Neimat, and R. J. Webster, "Concentric tube robots as steerable needles: Achieving follow-the-leader deployment," *IEEE Transactions on Robotics*, vol. 31, no. 2, pp. 246–258, 2015.

[13] R. Xu, A. Asadian, S. F. Atashzar, and R. V. Patel, "Real-time trajectory tracking for externally loaded concentric-tube robots," in *2014 IEEE International Conference on Robotics and Automation (ICRA)*, 2014, pp. 4374–4379.

[14] Y. Lu, C. Zhang, S. Song, and M. Q. . Meng, "Precise motion control of concentric-tube robot based on visual servoing," in *2017 IEEE International Conference on Information and Automation (ICIA)*, 2017, pp. 299–304.

[15] A. V. Kudryavtsev, M. T. Chikhaoui, A. Liadov, P. Rougeot, F. Spindler, K. Rabenorosoa, J. Burgner-Kahrs, B. Tamadazte, and N. Andreff, "Eye-in-hand visual servoing of concentric tube robots," *IEEE Robotics and Automation Letters*, vol. 3, no. 3, pp. 2315–2321, 2018.

[16] M. Mahvash and P. E. Dupont, "Stiffness control of surgical continuum manipulators," *IEEE Transactions on Robotics*, vol. 27, no. 2, pp. 334–345, 2011.

[17] K. Leibrandt, C. Bergeles, and G. Z. Yang, "Implicit active constraints for safe and effective guidance of unstable concentric tube robots," in *2016 IEEE/RSJ International Conference on Intelligent Robots and Systems (IROS)*, 2016, pp. 1157–1163.

[18] B. Siciliano, "Kinematic control of redundant robot manipulators: A tutorial," *Journal of Intelligent and Robotic Systems*, vol. 3, no. 3, pp. 201–212, 1990.

[19] C. R. Carignan, "Trajectory optimization for kinematically redundant arms," *Journal of Robotic Systems*, vol. 8, no. 2, pp. 221–248, 1991.

[20] S. Sra, "A new metric on the manifold of kernel matrices with application to matrix geometric means," in *Advances in Neural Information Processing Systems 25*, F. Pereira, C. J. C. Burges, L. Bottou, and K. Q. Weinberger, Eds. Curran Associates, Inc., 2012, pp. 144–152.

[21] J. Nocedal and S. J. Wright, *Numerical Optimization*. New York, NY: Springer New York, 2006, pp. 135–163.

[22] K. Leibrandt, C. Bergeles, and G. Z. Yang, "Implicit active constraints for concentric tube robots based on analysis of the safe and dexterous workspace," in *2017 IEEE/RSJ International Conference on Intelligent Robots and Systems (IROS)*, 2017, pp. 193–200.

[23] S. Chiaverini, B. Siciliano, and O. Egeland, "Review of the damped least-squares inverse kinematics with experiments on an industrial robot manipulator," *IEEE Transactions on Control Systems Technology*, vol. 2, no. 2, pp. 123–134, 1994.

[24] M. Quigley, K. Conley, B. Gerkey, J. Faust, T. Foote, J. Leibs, R. Wheeler, and A. Y. Ng, "Ros: an open-source robot operating system," in *ICRA workshop on open source software*, vol. 3, no. 3.2. Kobe, Japan, 2009, p. 5.

[25] G. Bradski and A. Kaehler, "Opencv," *Dr. Dobbs journal of software tools*, vol. 3, 2000.